

Weakly-supervised Transfer for 3D Human Pose Estimation in the Wild

Xingyi Zhou¹, Qixing Huang², Xiao Sun³, Xiangyang Xue¹, Yichen Wei³

¹Shanghai Key Laboratory of Intelligent Information Processing
School of Computer Science, Fudan University

²The University of Texas at Austin

³Microsoft Research

{zhouxy13, xyxue}@fudan.edu.cn, huangqx@cs.utexas.edu, {xias, yichenw}@microsoft.com

Abstract

In this paper, we study the task of 3D human pose estimation in the wild. This task is challenging because existing benchmark datasets provide either 2D annotations in the wild or 3D annotations in controlled environments.

We propose a weakly-supervised transfer learning method that learns an end-to-end network using training data with mixed 2D and 3D labels. The network augments a state-of-the-art 2D pose estimation network with a 3D depth regression network. Unlike previous approaches that train these two sub-networks in a sequential manner, we introduce a unified training method that fully exploits the correlation between these two sub-tasks and learns common feature representations. In doing so, the 3D pose labels in controlled environments are transferred to images in the wild that only possess 2D annotations. In addition, we introduce a 3D geometric constraint to regularize the prediction 3D poses, which is effective on images that only have 2D annotations.

Our method leads to considerable performance gains and achieves competitive results on both 2D and 3D benchmarks. It produces high quality 3D human poses in the wild, without supervision of in-the-wild 3D data.

1. Introduction

Human pose estimation is an important task in computer vision with numerous applications in human-computer interaction, virtual reality, and action understanding. Existing research in human pose estimation falls into two categories: 2D human pose estimation and 3D human pose estimation. 2D human pose estimation aims at detecting the pixel coordinates of the joints of an underlying human skeleton. Thanks to the availability of large-scale 2D annotated human poses and the emergence of deep neural networks, this problem has gained tremendous success re-

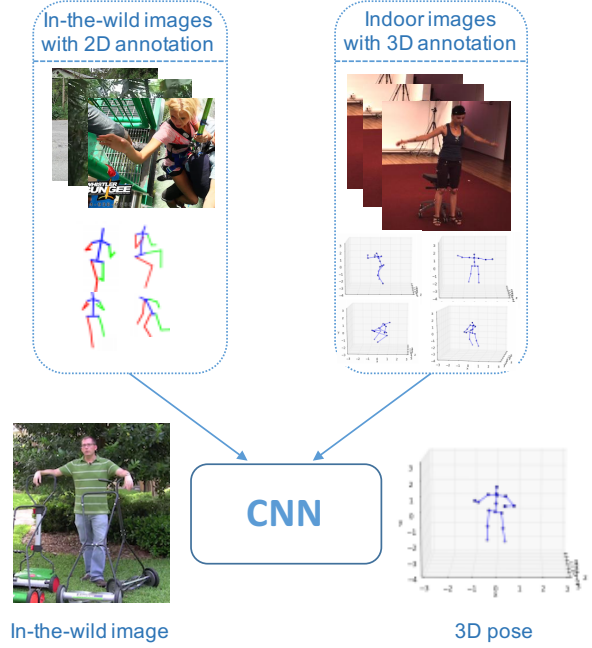


Figure 1. A schematic illustration of our method: transferring 3D annotation from indoor images to in-the-wild images. Top (Training): Both indoor images with 3D annotation (Right) and in-the-wild images with 2D annotation (Left) are used to train the deep neural network. Bottom (Testing): The learned network can predict the 3D pose of the human in in-the-wild images.

cently [18, 29, 12, 5, 8]. State-of-the-art techniques are able to achieve accurate predictions across a wide range of settings (e.g., on images in the wild [2]).

In contrast to 2D human pose estimation, advances in 3D human pose estimation remain rather limited. This is due to the fact that 3D human pose estimation may be ambiguous (multiple possible 3D poses from a single image). Moreover, it is extremely difficult to collect 3D pose annotations at scale. As a result, there is no 3D human pose

estimation benchmark dataset for images in the wild. Instead, commonly used 3D datasets [13, 24] were captured by mocap systems in restricted indoor environments. Deep neural networks [14, 33] trained on these datasets do not generalize well to images in the wild.

Previous methods for 3D human pose estimation in the wild usually proceed in two sequential steps [34, 26, 6, 3, 30, 31]. The first step estimates 2D joint locations [18, 29, 12], and the second step recovers 3D pose from these 2D joints [21, 32, 1]. In this way, each step can be trained using existing datasets. Namely, 2D joint predictions are trained from 2D annotations in the wild, while 3D pose recovery from 2D joints is trained from existing 3D MoCap data. However, such a sequential methodology is sub-optimal because the original in-the-wild 2D image information, which provides rich cues for 3D pose recovery, is discarded in the second step.

Recently, Mehta et al. [16] has shown that 2D-to-3D knowledge transfer, i.e., using pre-trained weights of 2D pose networks to initialize 3D pose regression networks can significantly improve 3D pose estimation performance. This indicates that the 2D and 3D pose estimation tasks are inherently entangled and share common representations.

In this work, we argue that the inverse knowledge transfer, i.e., from 3D annotations of indoor images to in-the-wild images, offers an effective solution for 3D pose prediction in the wild. We introduce an unified framework, where 2D annotations of in-the-wild images serve as weak labels for the 3D pose estimation task. In other words, we consider a weakly-supervised transfer problem, where the source is fully annotated images in restricted indoor environment and the target is weakly-labeled images in the wild.

We propose an end-to-end network for solving this weakly-supervised transfer problem. Similar to previous works [34, 26, 6, 3, 30, 31], our network consists of a 2D module and a 3D module. However, instead of merely feeding the output of the 2D module as input to the 3D module, a key feature of the proposed network is to connect the 3D module with the intermediate layers of the 2D module. This allows us to share common representations between the 2D and the 3D tasks. The network is trained end-to-end with both 2D and 3D data in the same mini-batch. For the weakly-labeled in-the-wild images, we introduce a geometric constraint for training the 3D pose network. This geometric constraint is based on the observation that relative bone lengths in a human skeleton remain approximately fixed. In our experiments, we found this constraint provides an effective regularization when adapting the 3D pose information from labeled images in indoor environments to unlabeled images in the wild.

Our contributions are summarized as following:

- For the first time, we propose an end-to-end 3D human pose estimation framework that produces 3D pose for

in-the-wild images. Our framework achieves state-of-the-art performance on several benchmarks, with a unified model. Towards solid and quantitative evaluation, we also annotated the 3D poses of MPII validation image set, using a semi-automatic annotation procedure.

- We propose a 3D geometric constraint-based loss for 3D pose estimation from images with only 2D joint annotations.

Code is publicly available at <https://github.com/xingyizhou/pose-hg-3d>.

2. Related Work

Human pose estimation has been studied considerably in the past [17, 23], and it is beyond the scope of this paper to provide a complete overview of the literature. In this section, we focus on single image 3D human pose estimation literature which is most relevant to the context of this paper. We will also discuss related works on imposing weakly-/un-supervised constraints for training neural networks.

3D Human Pose Estimation. Given well labeled data (e.g., 3D joint locations of a human skeleton [13, 24]), 3D human pose estimation can be formulated as a standard supervised learning problem. A popular approach is to train a neural network to directly regress joint locations [14]. Recently, people have generalized this approach in different directions. Zhou et al. [33] propose to explicitly enforces the bone-length constraints in the prediction, using a generative forward-kinematic layer; Tekin et al. [25] embed an pre-trained auto-encoder at the top of the network. In contrast these works, Pavlakos et al introduce a 3D convolution approach, by regressing a volumetric representation of 3D skeleton [20]. Despite the performance gain on standard 3D pose estimation benchmark datasets, the resulting networks do not generalize to images in the wild due to the domain difference between natural images and the specific capture environments utilized by these benchmark datasets.

A standard approach to address the domain difference between 3D human pose estimation datasets and images in the wild is to split the task into two separate sub-tasks [34, 26, 6, 3, 30]. The first task estimates 2D joint locations. This sub-task can utilize any existing 2D human pose estimation method (e.g., [18, 29, 12, 5]) and can be trained from images in-the-wild datasets. The second task regresses the 3D locations of these 2D joints. Since the input at this step is just a set of 2D locations, the 3D pose estimation network can be trained on any benchmark datasets and then adapted in other settings. Regarding 3D pose estimation from 2D joint locations, [34] use an EM algorithm to find a 3D skeleton obtained by the combination of a sparse dictionary from the 2D heat-map; [30, 20] use 3D pose data and its 2D projection to train a heatmap-to-3D

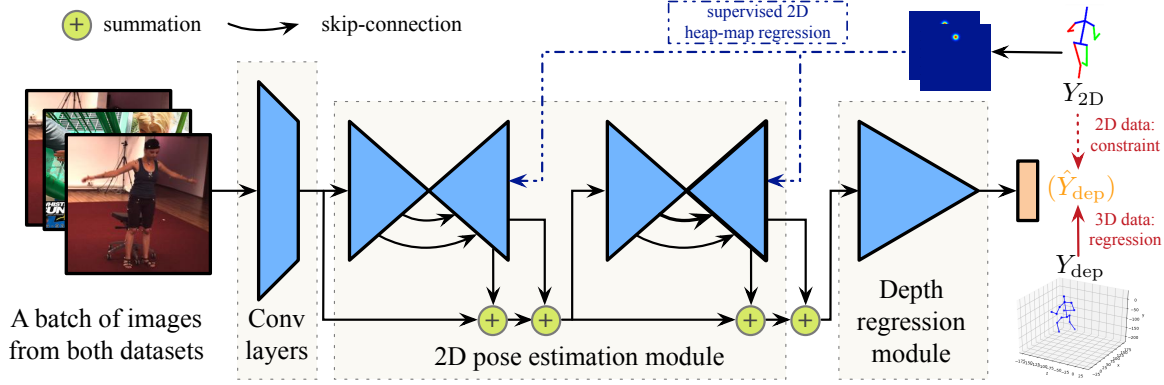


Figure 2. Illustration of our framework: In testing, images go through the stacked hourglass network and turn into 2D heat-maps. The 2D heat-maps and with lower-layer images features are summed as the input of the following depth regression module. In training, images from both 2D and 3D datasets are mixed in a single batch. For the 3D data, the standard regression with Euclidean Loss is applied. For the 2D data, we propose a weakly-supervised loss based on its 2D annotation and prior knowledge of human skeleton.

pose network without the original image; Bogo et al. [3] optimize both the pose and shape terms of a linear 3D human model [15] to best fit its 2D projection; Chen et al. [6] use nearest-neighbor search to match the estimated 2D pose to a 3D pose as well as a camera-view which may produce a similar 2D projection from a large 3D pose library; finally, Tome et al. [26] propose a pre-trained probabilistic 3D pose model layer that first generates plausible 3D human model from 2D heat-maps, and then refines these heat maps by combining 3D pose projection and the image features. All these methods, however, share a common limitation: the 3D pose is only estimated from the 2D joints, which is known to produce ambiguous results. In contrast, our approach leverages both 2D joint locations as well as intermediate feature representations from the original image.

An alternative approach for 3D human pose estimation is to train from synthetic datasets which are generated from deforming a human template model with known 3D ground truth [7, 22]. This is indeed a viable solution, but the fundamental challenge is how to model the 3D environment so that the distribution of the synthesized images matches that of the natural images. It turns out state-of-the-art methods along this line are less competitive on natural images.

Weakly-/un-supervised constraints. In the presence of insufficient training data, incorporating generic or weakly supervised constraints among the prediction serves as a powerful tool for performance boosting. This idea was usually utilized in image classification or segmentation. Pathak et al. [19] propose a constrained optimization framework that utilizes a linear constraint over sum of label probabilities for weakly supervised semantic segmentation. Tzeng et al. [28] propose a domain confusion loss to maximize the confusion between two datasets so as to encourage a

domain-invariant feature. Recently, Hoffman et al. [11] introduce an adversarial learning based global domain alignment method and utilize a weak label constraint to apply fully connected networks in the wild. In this paper, we show this general concept can be used for pose estimation as well. To best of our knowledge, our approach is the first to leverage geometry-guided constraint to regularize the pose estimation network for images in the wild.

3. Approach

3.1. Overview

Given an RGB image I containing a human subject, we aims to estimate its 3D pose $Y \in \mathcal{Y}_{3D}$, represented by its 3D joint coordinates of a pre-defined human skeleton, i.e. $\mathcal{Y}_{3D} \in \mathcal{R}^{J \times 3}$, where J is the number of joints. We follow the convention of representing each 3D coordinate in the local camera coordinate system associated with I , namely, the first two coordinates are given by image coordinates (which define the corresponding 2D joint location), and the third coordinate is the *depth* of this 2D joint.

We propose an end-to-end neural network for 3D pose recovery (See Fig. 2). The network consists of a 2D pose estimation module (Section 3.2) and a depth regression module (Section 3.3). Given an input image, the 2D pose estimation module predicts its 2D joint locations $Y_{2D} \in \mathcal{Y}_{2D}$, where $\mathcal{Y}_{2D} \subset \mathcal{R}^{J \times 2}$, and the depth regression module outputs their depth values $Y_{dep} \in \mathcal{Y}_{dep}$, where $\mathcal{Y}_{dep} \subset \mathcal{R}^{J \times 1}$. The final output is the concatenation of Y_{2D} and Y_{dep} .

We show how to train the network from both 3D pose data (where we have ground-truth labels for both the 2D joints \mathcal{Y}_{2D} and the depth values \mathcal{Y}_{dep}) and images in the wild (where we only have ground-truth labels for 2D joints \mathcal{Y}_{2D}).

In the reminder of this section, we denote the 3D and 2D training image sets as \mathcal{I}_{3D} and \mathcal{I}_{2D} , respectively.

3.2. 2D Pose Estimation Module

We adapt the state-of-the-art 2D human pose estimation network described in [18] as our 2D pose estimation module. Its output is represented as low-resolution heat-maps, each of which representing 2D probability distribution of the corresponding joint $\hat{Y}_{HM} \in \mathcal{R}^{H \times W}$. The prediction of each 2D pose $\hat{Y}_{2D} \in \mathcal{Y}_{2D}$ is given by the peak locations of these heat-maps. This heat-map representation is beneficial for its feasibility to combine (concatenate or sum) with the lower-layer image features for designing the input to depth regression module (as shown in Fig 2). We model the training objective of this part as

$$L_{2D}(\hat{Y}_{HM}, Y_{2D}) = \sum_h \sum_w (\hat{Y}_{HM}^{(h,w)} - G(Y_{2D})^{(h,w)})^2. \quad (1)$$

In other words, it measures the L^2 distance between the predicted heat-maps \hat{Y}_{HM} and the heat-maps $G(Y_{2D})$ rendered from the ground truth Y_{2D} through a Gaussian kernel [18].

3.3. Depth Regression Module

Compared with previous methods that regress 3D joint locations from 2D joint predictions, our approach innovates in terms of (i) network design with the integration of 2D and 3D modules, and (ii) training with a 3D geometric constraint induced loss. The details are given below:

Integration of 2D and 3D modules. The purpose of the depth regression module is to predict the depth $\hat{Y}_{dep} \in \mathcal{Y}_{dep}$ of each 2D joint. A critical design choice is what input features to utilize. A widely used strategy [34, 26, 6] is to take the 2D joint locations as the only input to predict their depth values so they can utilize the Mocap-only data. However, this method could lead to ambiguous results, as there may exist multiple 3D interpretations of a single 2D skeleton. We propose to combine 2D joint heat-maps and intermediate feature representations of the 2D pose estimation network as input to the depth regression module. These features, which extract semantic image features at multiple levels, provide additional cues for 3D pose recovery. Another consequence of utilizing these connections is to force a common feature representation between the 2D pose module and the 3D pose module.

3D geometric constraint induced loss. The technical challenge of defining the training loss for the depth regression module is to integrate both fully-labeled and weakly-labeled images. In presence of a fully-annotated 3D dataset $\mathcal{S}_{3D} = \{\mathcal{I}_{3D}, \mathcal{Y}_{2D}, \mathcal{Y}_{dep}\}$, we can define the loss term by penalizing the predicted depth and the ground-truth depth with a standard Euclidean Loss. When weakly-labeled dataset $\mathcal{S}_{2D} = \{\mathcal{I}_{2D}, \mathcal{Y}_{2D}\}$ is present, we propose a geometric

constraint on the predicted depth. This geometric constraint provides an effective regularization for the predicted depth.

Specifically, suppose \hat{Y}_{dep} denote the predicted depth. We model the loss for the depth regression module as

$$L_{dep}(\hat{Y}_{dep}|I, Y_{2D}) = \begin{cases} \lambda_{reg} \|\hat{Y}_{dep} - Y_{dep}\|^2, & \text{if } I \in \mathcal{I}_{3D} \\ \lambda_{geo} L_{geo}(\hat{Y}_{dep}|Y_{2D}), & \text{if } I \in \mathcal{I}_{2D} \end{cases} \quad (2)$$

where λ_{reg} and λ_{geo} are the corresponding loss weights. $L_{geo}(\hat{Y}_{dep}|Y_{2D})$ is a geometry-guided loss described below.

This geometric term is based on the fact that ratios between bone lengths remain relative fixed in a human skeleton (e.g., upper/lower arms have a fixed length ratio, left/right shoulder bones share the same length). Specifically, let R_i be a set of involved bones in a skeleton group i , e.g. $R_{arm} = \{\text{left upper arm, left lower arm, right upper arm, right lower arm}\}$, and let l_e be the length of bone e . With \bar{l}_e we denote the length of bone e in a canonical skeleton. Then it is easy to see that $\frac{l_e}{\bar{l}_e}$ in a group R_i should remain fixed. We thus define the weakly-supervised loss to minimize the sum of variance among $\{\frac{l_e}{\bar{l}_e}\}_{e \in R_i}$ of each R_i :

$$L_{geo}(\hat{Y}_{dep}|Y_{2D}) = \sum_i \frac{1}{|R_i|} \sum_{e \in R_i} \left(\frac{l_e}{\bar{l}_e} - \bar{r}_i \right)^2, \quad (3)$$

where

$$\bar{r}_i = \frac{1}{|R_i|} \sum_{e \in R_i} \frac{l_e}{\bar{l}_e}.$$

Note that the bone length is a function of joint locations, which are functions on the predicted depths. This means Equation. 3 provides a regularization on the predicted depth. It is obvious that L_{geo} is continuous and differentiable with respect to \hat{Y}_{dep} . The specific equations for feed-forward and back-propagation are provided in the Supplemental material.

In our experiments, we consider 4 groups of bones: $R_{arm} = \{\text{left/right lower/upper arms}\}$, $R_{leg} = \{\text{left/right lower/upper legs}\}$, $R_{shoulder} = \{\text{left/right shoulder bones}\}$, $R_{hip} = \{\text{left/right hip bones}\}$. In contrast, we do not include body bones which tend to exhibit relatively high variance in bone length across different human shapes. Note that bones in different sets do not affect each other. The canonical human skeleton is set as the average of all training subjects of the 3D dataset in our experiments.

3.4. Training

We proceed to describe how to train the proposed network. Combining (1), (2), and (3), we model the loss term for each training image $I \in \mathcal{I}_{2D} \cup \mathcal{I}_{3D}$ as

$$L(\hat{Y}_{HM}, \hat{Y}_{dep}|I) = L_{2D}(\hat{Y}_{HM}, Y_{2D}) + L_{dep}(\hat{Y}_{dep}|I, Y_{2D}) \quad (4)$$

We employ stochastic gradient descent for training. Similar to [28] and [11], the mini-batch used at each iteration integrates both the 2D and 3D training data. In all of our experiments, the ratio between each type of training instances is 1, i.e., 50% of the instances in a mini-batch are images with 3D pose labels and the other 50% of the instances are images with only 2D pose labels. Regarding network training, a naive approach is to simultaneously train all the network components from scratch. However, we found this approach did not work well in practice, and it is important to provide proper initializations for each network component.

Instead, we train the proposed network using a three-stage training scheme, where the result of the previous stage provides an initialization for the next stage. The first stage initializes the 2D pose module using 2D annotated images described in [18].

The second stage initializes the 3D pose estimation module and fine-tunes the 2D pose estimation module. In this stage, we utilize both 2D and 3D annotated data for training except that we do not activate the geometric constraint (the weak supervision), i.e., set $\lambda_{geo} = 0$ in Equation 2.

The final stage fine-tunes the whole network with both 2D and 3D training data as well as the weak supervision induced from the geometric constraint. Note that we only use the geometric constraint in the third stage since it is highly non-convex, making it less effective when the 3D pose module is not sufficiently optimized.

4. 3D Annotation for MPII Validation Set

Annotating 3D pose manually is very challenging and has been rarely done in previous works [4]. To evaluate the effectiveness of 3D pose estimation in the wild quantitatively, MPII validation set [2, 27] is annotated in this work.

we propose a human-computer collaborating method to annotate the 3D pose more effectively and efficiently than purely manual annotation. The annotating method is based on the fact that the ratios between bone lengths in a human skeleton are relatively fixed. Employing this constraint greatly reduces the amount of manual annotations and simplifies the annotation process.

To annotate an image, we first run a state-of-the-art 3D pose reconstruction method [32] with ground truth 2D joints. The result is a set of independent joints. They serve as an initialization for annotation. These joints are rectified by a Kinematic Model [33] with an gradient-based optimization algorithm for its global scale, location, orientation and joint angles. The result is a 3D skeleton that best matches the initial joints and keeps the kinematic structure.

A human annotator then checks the validity of the optimized pose. In particular, if the inward or outward order is incorrect for each adjacent joint pair, the human annotator reverses the order by a simple command. Occasionally, the annotator can move the 3D joints with the constraint that

their projections are aligned with the 2D ground truth joints.

The optimization algorithm is automatically triggered whenever a human operation is performed. This ensures that the 3D skeleton model is always aligned with the human inputs. Human interactions and pose optimization are iterated until the annotator finds that the resulting pose is satisfactory. Annotating one image takes approximately one minute. Please refer to the supplemental material for snapshots of annotated 3D poses.

5. Experimental Evaluation

In this section, we provide experimental evaluations of our approach. We train a single model utilizing Human3.6M [13] and MPII [2] and evaluate on three different testing sets. We evaluate our method in two aspects: supervised 3D human pose estimation (Section 5.2) and transferred 3D human pose estimation in the wild (Section 5.3). Qualitative results are summarized in Table. 5, more qualitative results on MPII validation set can be found in the supplementary material.

5.1. Experimental Setup

5.1.1 Implementation Detail

Our method was implemented with torch7 [9]. The hourglass component was based on the released code of [18]. For the purpose of fast training, we used a shallow version of stacked hourglass, i.e. 2 stacks with 2 residual modules [10] for each hourglass. The depth regression regression module is a $4 \times$ conv & pooling network, which can be regarded as a half hourglass. The same network architecture and training iterations are used in all of our experiments. The first training stage in Section 3.4 took 240k with a batchsize of 6. This gave us a 2D pose estimation module with similar performance as described in [18]. Stage 2 and stage 3 took 200k and 40k iterations, respectively. The whole training procedure took about two days in one Titan X GPU with CUDA 8.0 and cudnn 5. A forward pass at testing is about 30ms, which means the system runs in real-time. We set $\lambda_{reg} = 0.1$ and $\lambda_{geo} = 0.01$ to match the magnitude and keep the 2D pose estimation task primal. We followed [18] to set all other hyper-parameters.

5.1.2 Datasets & Metrics

MPII. MPII dataset [2] is used for training. It is a large scale in-the-wild human pose dataset. The images are collected from on-line videos and annotated by human for $J = 16$ 2D joints. It contains 25k training images and 2957 validation images [27]. The human subjects are annotated with bounding boxes.

Human3.6M. Human 3.6M dataset [13] is used both in training and testing. It is a widely used dataset for 3D hu-

	Directions	Discussion	Eating	Greeting	Phoning	Photo	Posing	Purchases
Chen & Ramanan [6]	89.87	97.57	89.98	107.87	107.31	139.17	93.56	136.09
Tome et al. [26]	64.98	73.47	76.82	86.43	86.28	110.67	68.93	74.79
Zhou et al. [35]	87.36	109.31	87.05	103.16	116.18	143.32	106.88	99.78
Metha et al. [16]	59.69	69.74	60.55	68.77	76.36	85.42	59.05	75.04
Pavlakos et al. [20]	58.55	64.56	63.66	62.43	66.93	70.74	57.72	62.51
3D/wo geo	73.25	79.17	72.35	83.90	80.25	81.86	69.77	72.74
3D/w geo	72.29	77.15	72.60	81.08	80.81	77.38	68.30	72.85
3D+2D/wo geo	55.17	61.16	58.12	71.75	62.54	67.29	54.81	56.38
3D+2D/w geo	54.82	60.70	58.22	71.41	62.03	65.53	53.83	55.58
	Sitting	SittingDown	Smoking	Waiting	WalkDog	Walking	WalkPair	Average
Chen & Ramanan [6]	133.14	240.12	106.65	106.21	87.03	114.05	90.55	114.18
Tome et al. [26]	110.19	172.91	84.95	85.78	86.26	71.36	73.14	88.39
Zhou et al. [35]	124.52	199.23	107.42	118.09	114.23	79.39	97.70	79.9
Metha et al. [16]	96.19	122.92	70.82	68.45	54.41	82.03	59.79	74.14
Pavlakos et al. [20]	76.84	103.48	65.73	61.56	67.55	56.38	59.47	66.92
3D/wo geo	98.41	141.60	80.01	86.31	61.89	76.32	71.47	82.44
3D/w geo	93.52	131.75	79.61	85.10	67.49	76.95	71.99	80.98
3D+2D/wo geo	74.79	113.99	64.34	68.78	52.22	63.97	57.31	65.69
3D+2D/w geo	75.20	111.59	64.15	66.05	51.43	63.22	55.33	64.90

Table 1. Results of Human3.6M Dataset. The numbers are mean Euclidean distance(mm) between the ground-truth 3D joints and the estimations of different methods.

man pose estimation. This dataset contains 3.6 millions of RGB images captured by a MoCap System in an indoor environment. We down-sampled the video from 50fps to 10fps for both the training and testing sets to reduce redundancy. Following the standard protocol in [14, 34, 33], we use 5 subjects(S1, S5, S6, S7, S8) for training and the rest 2 subjects(S9, S11) for testing. The evaluation metric is mean per joint position error(MPJPE) in mm after aligning the depths of the root joints. We use its projected 2D locations for training the 2D module and its depth annotation for depth regression module.

MPI-INF-3DHP. MPI-INF-3DHP [16] is a newly proposed 3D human pose dataset. The images were captured by a MoCap system both in indoor and outdoor scenes. We use the test set of MPI-INF-3DHP only for experimental evaluation. The test set contains 2929 valid frames from 6 subjects, performing 7 actions. Following [16], we employ average PCK (with a threshold 150mm) and AUC as the evaluation metrics, i.e., after aligning the root joint (pelvis). Note that we assume the global scale is known for experimental evaluation. We observe that the definition of pelvis position in MPI-INF-3DHP is different from the one used in our training sets (i.e., Human 3.6M and MPII), so we moved the pelvis and hips towards neck in a fixed ratio (0.2) as post processing in our evaluation.

MPII-Validation-3D. As described in section 4, we

manually annotated the 3D joint positions for the MPII validation set [27]. In total, this dataset collects 1799 images, providing a more comprehensive dataset than MPI-INF-3DHP [16] for evaluating 3D human pose prediction in the wild. In terms of the evaluation protocol, we report statistics of 3D joint position error(MPJPE) in pixels, where the input images are resized to 256×256 .

5.1.3 Baseline Setup

We consider three baselines for ablation studies. They are used to evaluate different aspects of our approach.

3D/wo geo is a plain implementation of our network architecture. More precisely, it only uses 3D labeled data to train the network, and the in-the-wild images are not used. Note that the 2D hourglass is pre-trained on the 2D dataset.

3D/w geo adds the geometric constraint on the first baseline method. i.e., when regressing the depth values, we explicitly penalizes the variance among the selected bone sets.

3D+2D/wo geo trains the network with both 3D and 2D datasets in a single mini-batch. The only difference between this method and the proposed full pipeline is that the geometric constraint is not utilized for 2D labeled data when training the 3D module.

3D+2D/w geo is the full pipeline of our methods.

	Studio GS	Studio no GS	Outdoor	ALL PCK	AUC
Metha et al.(H36M+MPII) [16]	70.8	62.3	58.8	64.7	31.7
3D/wo geo	34.4	40.8	13.6	31.5	18.0
3D/w geo	45.6	45.1	14.4	37.7	20.9
3D+2D/wo geo	68.8	61.2	67.5	65.8	32.1
3D+2D/w geo	71.1	64.7	72.7	69.2	32.5
Metha et al.(MPI-INF-3DHP) [16]	84.1	68.9	59.6	72.5	36.9

Table 2. Results of MPI-INF-3DHP Dataset by scene. GS indicates green screen background. The results are shown in PCK and AUC.

	PCKh@0.5	MPJPE
GT 2D + Zhou et al. [32]	100%	15.98
Hourglass 2D + Zhou et al. [32]	87.92%	21.29
3D/wo geo	19.78%	64.28
3D+2D/wo geo	85.81%	21.33
3D+2D/w geo	86.06%	19.09

Table 3. Results of MPII-Validation-3D. The results are shown in 2D PCKh and MPJPE in 3D pixel.

	3D/wo geo	3D/w geo
Upper arm	6.27	4.80
Lower arm	10.11	6.64
Upper leg	6.89	4.93
Lower leg	8.03	6.22

Table 4. Evaluation of left-right Symmetry of with and without constraint. The results are shown in average L1 distance between left and right bone in 3D pixel.

5.2. Supervised 3D Human Pose Estimation

We first report and analyze the performance of our method on Human 3.6M dataset [13].

Baseline comparison. Table 1 compares the proposed approach with the three baseline approaches. The average MPJPE of the first baseline **3D/wo geo** is $82.44mm$. Note that this is already comparable to most state-of-the-art methods [33, 26, 35], indicating the effectiveness of our network architecture. This baseline is also in par with the proposed method of Metha et al. [16], which fine-tuned 2D pose network [12] with 3D data for information transfer. The difference is that we did not use $1000\times$ learning rate decay for the transferred layers, which in our case yielded worse performance.

Training with additional geometric constraint, i.e., **3D/w geo**, provides a decent performance gain. This shows our geometry constraint is consistent with the supervision signal.

Training with both 2D and 3D data (**3D+2D/wo geo**),

provides significant performance gain — average MPJPE dropped to $64.90mm$, which is superior to all existing state-of-the-art methods [16, 20]. This shows the advantage of using both data sources in a single batch, enabling direct fusion of features from both datasets.

Weakly supervised constraint **3D+2D/w geo** brings further accuracy improvements. Note that the constraints are applied on the disjoint 2D dataset, showing that the provided prior knowledge is universal. We have also tested adding constraints on 3D data. The results are similar.

Comparisons to other in the wild methods. Our method is superior to other methods that are applicable to in-the-wild images. Comparing to some two-step methods, MPJPE of Chen & Ramanan [6] is $114.18mm$ and MPJPE of Zhou et al. [35] is $79.9mm$. Pavlakos et al. [20] provided an alternative decoupled version which can also be applied in the wild, but its MPJPE increased to $78.1mm$. In contrast, MPJPE of our method is $64.90mm$, which is significantly better than all previous methods.

Intermediate 2D features improve 3D pose estimation.

We also conducted experiment on 3D pose reconstruction, i.e., recovering 3D pose from *ground truth* 2d points, to demonstrate the usefulness of the intermediate 2D features for 3D pose recovery. We replaced our 2D prediction with ground truth 2D joint locations, and the prediction error is $50.4mm$, which is better than the state-of-the-art 3D reconstruction methods ($53.2mm$ of Pavlakos et al. [20] and $55.6mm$ of Zhou et al. [35]). This shows the benefit of combining additional image features for 3D pose prediction.

5.3. Transferred Human Pose In the Wild

We evaluate the generalization of our method on two datasets captured in different in-the-wild environments.

5.3.1 MPI-INF-3DHP Dataset

The first dataset is MPI-INF-3DHP [16]. It exhibits considerable domain shift from both MPII and Human 3.6M datasets. Table 2 compares the performance of various methods on MPI-INF-3DHP. In this case, the first two baseline methods, i.e., **3D/wo geo** and **3D/w geo**, yielded low

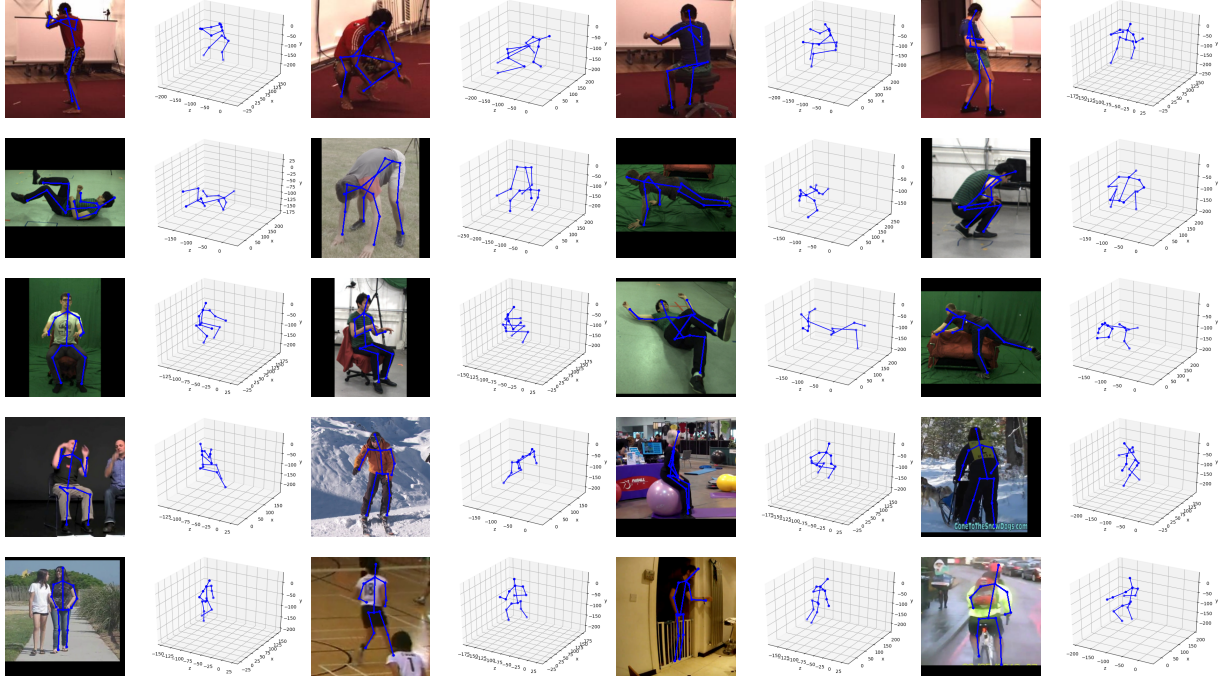


Table 5. Qualitative results from different datasets. We show the 2D pose on the original image and 3D pose from a novel view. First line: Human 3.6M dataset; Second and third lines: MPI-INF-3DHP dataset; Fourth and fifth lines: MPII dataset.

performance. This is not surprising, as the training set contains only indoor images. However, it is noticeable that even in this case, the one with the geometric constraint performs better than the un-constrained one.

3D+2D/wo geo achieved 65.8 and 32.1 in PCK and AUC, respectively. These numbers are better than their counterparts in [16] with Human 3.6M training data, again showing the advantage of our training scheme.

Our full pipeline yields 69.2 in PCK and 32.5 in AUC. These numbers are close to the one that is derived from the original training data of MPI-INF-3DHP [16], which has 72.5 in PCK and 36.5 in AUC. This confirms the ability of our method on in-the-wild images.

5.3.2 MPII Validation 3D Dataset

Finally, we evaluate our framework on MPII validation set, which is a complete in-the-wild human pose dataset.

State-of-the-art comparison. As for comparison to the state-of-the-art method, we combine the output of the hourglass network [18] and the pose estimation module in [32], which is the state-of-the-art method for 3D pose recovery from 2D joints. To put the comparison in perspective, we also report the performance of combining ground-truth 2D joints and [32]. For evaluation, we employ PCKh@0.5 and 3D MPJPE for 2D and 3D pose predictions, respectively.

As illustrated in Table 3, our proposed method has 19.09

in 3D MPJPE, which is superior to the state-of-the-art method that combines Hourglass [18] and [32] (which has 21.29 in 3D MPJPE). The 3D MPJPE of **3D+2D/wo geo** is 21.33. This shows the effectiveness of the geometric constraint on this dataset. Note that the 3D MPJPE of **3D/wo geo** is only 64.28. This means that utilizing in-the-wild training images and the proposed training scheme are crucial for in-the-wild 3D pose recovery.

Geometric validity. Another generic constraint on human skeleton is that the bone lengths of symmetric bones (e.g., left and right upper arms) should be identical to each other. We employ this constraint on upper/lower arms/legs to evaluate the quality of a prediction. As illustrated in Table 4, **3D+2D/wo geo** exhibits a considerable larger violation of bone length symmetry than utilizing the variance constraint for training. This provides another justification for the effectiveness of our weakly-supervised constraint.

2D accuracy versus 3D accuracy. We note that our method has a slightly low 2D joint accuracy than the output of the Hourglass model. This is expected as 2D joint accuracy is not the only training target in our method. However, utilizing the geometric constraint improves the 2D joint accuracy as well. This indicates that our network is able to propagate this geometric constraint from the 3D module to the 2D module, which justifies the design goal of our network.

6. Future Work and Conclusions

In this paper, we introduced an end-to-end system that combines 2D pose labels in the wild and 3D pose labels in restricted environments for the challenge problem of 3D human pose estimation in the wild. In the future, we plan to explore more un-/weakly-supervised constraints for a better transfer, e.g., a domain alignment network as in [11, 28]. We hope this work can inspire more works on un-/weakly-supervised transfer learning and on 3D human pose estimation in the wild.

References

- [1] I. Akhter and M. J. Black. Pose-conditioned joint angle limits for 3d human pose reconstruction. In *Proceedings of the IEEE Conference on Computer Vision and Pattern Recognition*, pages 1446–1455, 2015. 2
- [2] M. Andriluka, L. Pishchulin, P. Gehler, and B. Schiele. 2d human pose estimation: New benchmark and state of the art analysis. In *IEEE Conference on Computer Vision and Pattern Recognition (CVPR)*, June 2014. 1, 5
- [3] F. Bogo, A. Kanazawa, C. Lassner, P. Gehler, J. Romero, and M. J. Black. Keep it smpl: Automatic estimation of 3d human pose and shape from a single image. In *European Conference on Computer Vision*, pages 561–578. Springer, 2016. 2, 3
- [4] L. Bourdev and J. Malik. Poselets: Body part detectors trained using 3d human pose annotations. In *Computer Vision, 2009 IEEE 12th International Conference on*, pages 1365–1372. IEEE, 2009. 5
- [5] A. Bulat and G. Tzimiropoulos. Human pose estimation via convolutional part heatmap regression. In *European Conference on Computer Vision*, pages 717–732. Springer, 2016. 1, 2
- [6] C.-H. Chen and D. Ramanan. 3d human pose estimation= 2d pose estimation+ matching. *arXiv preprint arXiv:1612.06524*, 2016. 2, 3, 4, 6, 7
- [7] W. Chen, H. Wang, Y. Li, H. Su, Z. Wang, C. Tu, D. Lischinski, D. Cohen-Or, and B. Chen. Synthesizing training images for boosting human 3d pose estimation. In *3D Vision (3DV), 2016 Fourth International Conference on*, pages 479–488. IEEE, 2016. 3
- [8] X. Chu, W. Yang, W. Ouyang, C. Ma, A. L. Yuille, and X. Wang. Multi-context attention for human pose estimation. *arXiv preprint arXiv:1702.07432*, 2017. 1
- [9] R. Collobert, K. Kavukcuoglu, and C. Farabet. Torch7: A matlab-like environment for machine learning. In *BigLearn, NIPS Workshop*, 2011. 5
- [10] K. He, X. Zhang, S. Ren, and J. Sun. Deep residual learning for image recognition. In *Proceedings of the IEEE Conference on Computer Vision and Pattern Recognition*, pages 770–778, 2016. 5
- [11] J. Hoffman, D. Wang, F. Yu, and T. Darrell. Fcns in the wild: Pixel-level adversarial and constraint-based adaptation. *arXiv preprint arXiv:1612.02649*, 2016. 3, 5, 9
- [12] E. Insafutdinov, L. Pishchulin, B. Andres, M. Andriluka, and B. Schiele. Deeppercut: A deeper, stronger, and faster multi-person pose estimation model. In *European Conference on Computer Vision*, pages 34–50. Springer, 2016. 1, 2, 7
- [13] C. Ionescu, D. Papava, V. Olaru, and C. Sminchisescu. Human3.6m: Large scale datasets and predictive methods for 3d human sensing in natural environments. *IEEE Transactions on Pattern Analysis and Machine Intelligence*, 36(7):1325–1339, jul 2014. 2, 5, 7
- [14] S. Li and A. B. Chan. 3d human pose estimation from monocular images with deep convolutional neural network. In *Asian Conference on Computer Vision*, pages 332–347. Springer, 2014. 2, 6
- [15] M. Loper, N. Mahmood, J. Romero, G. Pons-Moll, and M. J. Black. Smpl: A skinned multi-person linear model. *ACM Transactions on Graphics (TOG)*, 34(6):248, 2015. 3
- [16] D. Mehta, H. Rhodin, D. Casas, O. Sotnychenko, W. Xu, and C. Theobalt. Monocular 3d human pose estimation using transfer learning and improved cnn supervision. *arXiv preprint arXiv:1611.09813*, 2016. 2, 6, 7, 8
- [17] T. B. Moeslund and E. Granum. A survey of computer vision-based human motion capture. *Computer vision and image understanding*, 81(3):231–268, 2001. 2
- [18] A. Newell, K. Yang, and J. Deng. Stacked hourglass networks for human pose estimation. In *European Conference on Computer Vision*, pages 483–499. Springer, 2016. 1, 2, 4, 5, 8
- [19] D. Pathak, P. Krahenbuhl, and T. Darrell. Constrained convolutional neural networks for weakly supervised segmentation. In *Proceedings of the IEEE International Conference on Computer Vision*, pages 1796–1804, 2015. 3
- [20] G. Pavlakos, X. Zhou, K. G. Derpanis, and K. Daniilidis. Coarse-to-fine volumetric prediction for single-image 3d human pose. *arXiv preprint arXiv:1611.07828*, 2016. 2, 6, 7
- [21] V. Ramakrishna, T. Kanade, and Y. Sheikh. Reconstructing 3d human pose from 2d image landmarks. In *European Conference on Computer Vision*, pages 573–586. Springer, 2012. 2
- [22] G. Rogez and C. Schmid. Mocap-guided data augmentation for 3d pose estimation in the wild. In *Advances in Neural Information Processing Systems*, pages 3108–3116, 2016. 3
- [23] N. Sarafianos, B. Boteanu, B. Ionescu, and I. A. Kakadiaris. 3d human pose estimation: A review of the literature and analysis of covariates. *Computer Vision and Image Understanding*, 152:1–20, 2016. 2
- [24] L. Sigal, A. O. Balan, and M. J. Black. Humaneva: Synchronized video and motion capture dataset and baseline algorithm for evaluation of articulated human motion. *International journal of computer vision*, 87(1-2):4, 2010. 2
- [25] B. Tekin, I. Katircioglu, M. Salzmann, V. Lepetit, and P. Fua. Structured prediction of 3d human pose with deep neural networks. *arXiv preprint arXiv:1605.05180*, 2016. 2
- [26] D. Tome, C. Russell, and L. Agapito. Lifting from the deep: Convolutional 3d pose estimation from a single image. *arXiv preprint arXiv:1701.00295*, 2017. 2, 3, 4, 6, 7
- [27] J. Tompson, R. Goroshin, A. Jain, Y. LeCun, and C. Bregler. Efficient object localization using convolutional net-

- works. In *Proceedings of the IEEE Conference on Computer Vision and Pattern Recognition*, pages 648–656, 2015. 5, 6
- [28] E. Tzeng, J. Hoffman, T. Darrell, and K. Saenko. Simultaneous deep transfer across domains and tasks. In *Proceedings of the IEEE International Conference on Computer Vision*, pages 4068–4076, 2015. 3, 5, 9
- [29] S.-E. Wei, V. Ramakrishna, T. Kanade, and Y. Sheikh. Convolutional pose machines. In *Proceedings of the IEEE Conference on Computer Vision and Pattern Recognition*, pages 4724–4732, 2016. 1, 2
- [30] J. Wu, T. Xue, J. J. Lim, Y. Tian, J. B. Tenenbaum, A. Torralba, and W. T. Freeman. Single image 3d interpreter network. In *European Conference on Computer Vision*, pages 365–382. Springer, 2016. 2
- [31] H. Yasin, U. Iqbal, B. Kruger, A. Weber, and J. Gall. A dual-source approach for 3d pose estimation from a single image. In *Proceedings of the IEEE Conference on Computer Vision and Pattern Recognition*, pages 4948–4956, 2016. 2
- [32] X. Zhou, S. Leonardos, X. Hu, and K. Daniilidis. 3d shape estimation from 2d landmarks: A convex relaxation approach. In *Proceedings of the IEEE Conference on Computer Vision and Pattern Recognition*, pages 4447–4455, 2015. 2, 5, 7, 8
- [33] X. Zhou, X. Sun, W. Zhang, S. Liang, and Y. Wei. Deep kinematic pose regression. In *Computer Vision–ECCV 2016 Workshops*, pages 186–201. Springer, 2016. 2, 5, 6, 7
- [34] X. Zhou, M. Zhu, S. Leonardos, K. G. Derpanis, and K. Daniilidis. Sparseness meets deepness: 3d human pose estimation from monocular video. In *Proceedings of the IEEE Conference on Computer Vision and Pattern Recognition*, pages 4966–4975, 2016. 2, 4, 6
- [35] X. Zhou, M. Zhu, G. Pavlakos, S. Leonardos, K. G. Derpanis, and K. Daniilidis. Monocap: Monocular human motion capture using a cnn coupled with a geometric prior. *arXiv preprint arXiv:1701.02354*, 2017. 6, 7